145
Wing–Rotor Aerodynamic Interaction in Tiltrotor Aircraft

G. Droandi*, G. Gibertini*, M. Biava**

*Dipartimento di Ingegneria Aerospaziale – Politecnico di Milano
Via La Masa 34, 20156 Milano – Italy
** AgustaWestland-Politecnico Advanced Rotorcraft Center (AWPARC)
Via G. Durando 10, 20158 Milano – Italy
e–mail: droandi@aero.polimi.it

Keywords: Tiltrotor, Aerodynamic, Rotor.

Abstract

Aerodynamic interaction between wing and rotors of a tiltrotor aircraft can produce negative effects on its flight performance, both in helicopter mode and aircraft mode flight. A numerical and experimental research activity about the aerodynamic interference between rotor and wing in tiltrotor aircraft was started at Politecnico of Milano. At the beginning of the activity, the aircraft geometry was defined following the tilting wing concept, and numerical simulations have been used to help the design of the experimental test rig. The aerodynamic design of the blade shape is carried out by a multi–objective optimization based on a controlled elitist genetic algorithm and rotor performance and efficiency curves are reported. Numerical simulations based on the solver ROSITA are performed to estimate the wing download due to the interaction with the rotor wake in hover condition. Several wing configurations for different span–wise locations of the tilt section are tested and aerodynamic loads for the experimental test rig design are evaluated.

1 Introduction

Aerodynamic interaction between wing and rotors of a titlrotor aircraft can produce negative effects mainly on the helicopter mode flight performance. For example, when a tiltrotor aircraft takes off and lands vertically the rotor wake strikes the upper surface of the wing creating a download that is, in hover condition, in the order of $10\% - 15\%$ of the rotor thrust (see Ref. [1], [2]). Wing–rotor aerodynamic interaction can also affect negatively the aircraft mode flight performance and the conversion phase of a tiltrotor. It is clear that, in order to optimize the performance of a tiltrotor aircraft operating in helicopter mode, it is necessary to minimize the download reducing the interference between wing and rotors. In the same manner, to improve the performance in aircraft mode, the efficiency of the propeller can be increased reducing its diameter. However, in order to have acceptable hover performance, actual tiltrotors (V–22 Ospray and BA609) have large rotors that develop high wing–rotor interference and prevent the take–off and landing in aircraft mode.

Since 10 years ago the ERICA (Enhanced Rotorcraft Innovative Concept Achievement) concept (see Ref. [3]) has been the subject of several research projects founded by European Community to overcome existing tiltrotor limitations and to improve their performance. The peculiarities of the ERICA design are the relatively small size of the rotors diameter and the cabability to tilt external parts of the wing. The reduced rotor diameter implies an increment of the power required to hover however is necessary to allow for horizontal take–off and landing. Consequently the tilting wing is necessary to allow for helicopter mode flight with such small rotors (with an estimated download of about 1%). This kind of solution has other advantages as it improves the performance in aircraft mode and positively affects the width of the conversion corridor. In last years, ERICA concept has been widely studied under several points of view but many aspects of this non conventional tiltrotor, as same quite basic aspect of the aerodynamics of wing–rotor interaction, could be investigated more deeply for possible future evolutions and other future applications of the ERICA concept.

For these reasons, a research activity about the aerodynamic interference between rotor and wing in tiltrotor aircrafts has been started at Politecnico of Milano. Such problem is approached making use of both numerical and experimental modeling. A preliminary aircraft geometry has been developed in–house based on the tiltwing concept but not strictly reproducing the ERICA geometry because the aim of the study is more general. Numerical simulations have been used to get a first insight in the main phenomena associated with aerodynamic interference between wing and rotor, and numerical results have also been used to help the design of the experimental test rig. All the studies of this research make use of an half–model configuration where just one half–wing and one rotor are reproduced. In the first part of this paper the geometry of full–scale aircraft is taken into account. The aerodynamic design of the shape of the blades is presented and rotor performance and efficiency curves are also reported. In the second part, computational fluid dynamics (CFD) simulations are used to estimate the wing download caused by the interaction with the rotor wake in hover condition. Several wing configurations have been tested for different span–wise locations of the tilt section. As result a wing is defined to give the maximum aerodynamic performance in terms of download in hover. In the last part of the paper, experimental test rig for hover tests is briefly described.

2 Aircraft sizing

In order to specify the model geometry and flight conditions to be tested, same general data of the whole aircraft has been assumed, defining an aircraft in the same class of ERICA [3]. Consequently, a typical mission profile for this kind of aircraft has been identified on the point to point service (that is the connection between two urban areas, two oil rigs, ect.) taken from and to vertports. Operational requirements and design goals for the full–scale aircraft have been then defined within this framework and are listed in Tab. 1. Aircraft design weights have been estimated by mean of statistical approach [4] and [5] and are reported in Tab. 2.

The wing has a span of 15 m and it is defined as the distance between the rotor axles. All the tests (numerical and experimental) of this research make use of an half–model configuration were just one half–wing and one rotor with the nacelle are reproduced. The fuselage is not included so that the wing root lies on the aircraft symmetry plane. The wing is a trapezoidal untwisted wing, with NACA 64A221 section. The chord c varies linearly from 3 m at root to 2 m at tip (i.e. at the nominal extremity of the wing, ideally prolonged up to the rotor axle, as shown by the Fig. 1). The nacelle has a maximum diameter of 1 m and a lenght of 4.535 m. The rotor has 4 non linearly tapered twisted blades with a radius of 3.7 m. The blade shape is the result of a multi–objective optimization based on the algorithm NSGA–II [6].

	H/C mode	A/C mode
Passengers	20	22
Crew	2 pilots	2 pilots
Cruise altitude	–	7500 m
Cruise speed	140 m/s	170 m/s
Climb speed	10 m/s	–
Rotor speed	560 rpm	430 rpm
Range	1200 km	1500 km

Table 1: Aircraft Operational requirements.

	VTO	STO
Empty weight	7100 kg	7100 kg
Payload	2000 kg	2200 kg
Crew	200 kg	300 kg
Fuel	1600 kg	2000 kg
Gross wieght	10900 kg	11600 kg

Table 2: Aircraft design weights.

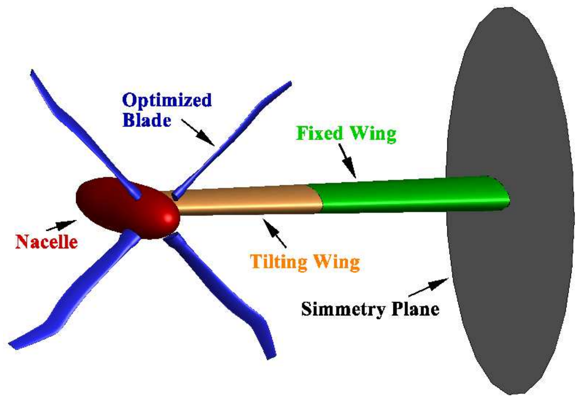

Figure 1: Aircraft model layout.

3 Blade project

The rotor blade aerodynamic design is a very critical task inside the project of a tiltrotor aircraft. For an aircraft of this class, the same propulsive system must be used both in helicopter and aircraft mode flight. Moreover, the required thrust for helycopter mode flight, that is more or less equal to half the weight of the aircraft in hover, is about five times the required thrust for aircraft mode flight, that corresponds to half the drag of the aircraft in forward flight. Nevertheless, a tiltrotor blade has to give good performance both in hover (and vertical climb) and forward flight. If the tiltrotor has a non conventional design, as in the case of ERICA, because it has the capability to take–off and land horizontally like an airplane, the rotor diameter has to be smaller than conventional ones (like V–22 Ospary and BA–609). All these requirements strongly influence the rotor design process and they have to be taken into account during the aerodynamic blade design. In general, this kind of problem can be seen like a shape optimization problem that can be efficiently approached by a genetic algorithm. In chapter 2 an aircraft in the same class of ERICA has been defined to study the aerodynamic interference between wing and rotor in a tiltrotor aircraft. The selected geometry does not exactly reproduce the ERICA one, thus only the main goals of the ERICA rotor system optimization have been considered to design a rotor blade able to fulfil the design requirements, neglecting for example the noise reduction problem.

3.1 Optimization problem definition

According to the main goals of the ERICA rotor system optimization and fixed the rotor radius (that is 3.7 m), the design points for the blade shape optimization have been chosen as follows:

- Objective 1: Maximization of the hover Figure of Merit (FM);
- Objective 2: Maximization of the Propulsive Efficiency (η_{climb}) in vertical climb;
- Objective 3: Maximization of the Propulsive Efficiency (η_{cruise}) in cruise at high speed.

The FM is calculated using the simple momentum theory (see Ref. [7] and [8]) and is defined as the ratio between the ideal power required to hover and the actual power required, that is:

$$FM = \frac{\text{Ideal power required to hover}}{\text{Actual shaft power required}} < 1, \quad (1)$$

where the ideal power is equal to $C_T^{3/2}/\sqrt{2}$ (momentum theory). Concerning the propulsive efficiency, Leishman and Rosen (see Ref. [8]) suggest for a tiltrotor aircraft the same definition adopted for conventional propellers, thus:

$$\eta = \frac{\text{Ideal propulsive power}}{\text{Actual shaft power required}}, \quad (2)$$

where the ideal propulsive power is TV_∞.

The previous points represent the objectives of the optimization process and they are supplied to the solver by a fitness function. Consequently the optimization process has been carried out on 3 different flight conditions related to the design points. Two different conditions were taken into account for the helicopter mode while only one for the aircraft mode (Tab. 3). To reduce the complexity of the optimization problem, it has been decided to choose the design rotor speed of each condition by comparison with rotor speeds of similar tiltrotors (XV-15, see ref. [9], V-22, see ref. [1], ERICA, see ref. [3]).

Condition 1	
Rotor speed	560 rpm
Altitude	0 m
Required thrust	$\frac{P^{VTO}_{MTOW}}{2}$
Condition 2	
Rotor speed	560 rpm
Altitude	0 m
Climb speed	10 m/s
Drag coefficient	1.5 [4]
Wing surface	35 m^2
Required thrust	$\frac{P^{VTO}_{MTOW}}{2} + \frac{D^{wb}}{2}$
Condition 3	
Rotor speed	430 rpm
Altitude	7500 m
Cruise speed	170 m/s
Drag coefficient	0.08 [4]
Wing surface	35 m^2
Required thrust	$\frac{D^{wb}}{2}$

Table 3: Flight conditions considered during the optimization process.

Since a tiltrotor blade has to work in very different flight conditions and it has to satisfy very different requirements, the blade shape optimization problem can be efficiently approached by the multi–objective optimization with a genetic algorithm. The blade shape is the result of a multi–variable, multi–objective constrained optimization based on a controlled elitist genetic algorithm founded on nondominated sorting genetic algorithm II (NSGA–II) [6], [10], that finds minima of multicomponent objective function using genetic algorithm. Nine positions along the blade radius have been chosen as optimization sections. For each station, design variables are the chord length (c), the twist angle (θ) and the airfoil shape (AS), thus the multi–objective optimization has been performed on a total number of 27 variables. The design variables array can be written as follows:

$$\mathbf{x} = (c_1, \ldots, c_9, \theta_1, \ldots, \theta_9, AS_1, \ldots, AS_9)\,. \qquad (3)$$

The objective function $\mathbf{f}(\mathbf{x})$ is an array composed by 3 different scalar objectives ($f_1(\mathbf{x})$, $f_2(\mathbf{x})$, $f_3(\mathbf{x})$) that are related to different flight conditions. The optimization problem may be written as follows:

Minimize:

$$\mathbf{f}(\mathbf{x}) = (f_k(\mathbf{x}))^T, \qquad \text{k=1,2,3} \qquad (4)$$

subject to:

$$\begin{aligned}
&c_n^{LB} \le c_n \le c_n^{UB}, && \text{n = 1,\ldots,9}\\
&\theta_n^{LB} \le \theta_n \le \theta_n^{UB}, && \text{n = 1,\ldots,9}\\
&AS_n^{LB} \le AS_n \le AS_n^{UB}, && \text{n = 1,\ldots,9}\\
&Aleq^{\theta}_{n,m}\theta_n \le 0, && \text{m = 1,\ldots,8}\\
&Aleq^{\theta}_{n,m}\theta_n \le b^{\theta}_m, && \text{m = 1,\ldots,8}\\
&Aleq^{c}_{n,m}c_n \le 0, && \text{m = 1,\ldots,8}\\
&Aleq^{c}_{n,m}c_n \le b^{c}_m, && \text{m = 1,\ldots,8}\\
&Aeq^{c}_{n,m}c_n = 0, && \text{m = 1,\ldots,8}\\
&\phi_{trim,k}(\mathbf{x}) = \mathbb{B}(\mathbf{x}, RC_k^{\infty}) && \text{k = 1,2,3}
\end{aligned}$$

In Eq. 4, constraints divide the search solution space into feasible and infeasible regions. Design variables are limited by a set of prescribed lower and upper bounds, so that a local Pareto set is found in the range $\mathbf{x}^{LB} \le \mathbf{x} \le \mathbf{x}^{UB}$. Linear inequality constraints limit the maximum twist angle variations and chord rate of change between one section and the following, while chord values of some sections are subject to linear equality constraints. FM in hovering flight and η_{climb} and η_{cruise} in axial flight are computed by an aerodynamic solver, based on the blade element momentum theory (BEMT) [7]. Aerodynamic characteristics of airfoil sections have been previously stored in tables for a wide range of angles of attack, Reynolds and Mach numbers. The aerodynamic solver extracts interpolated values of lift coefficient (C_l), drag coefficient (C_d) and pitching moment coefficient (C_m), for every specified values of angle of attack, Reynolds and Mach number inside the stored range. The aerodynamic solver includes wake swirl effects [11] and Prandtl's tip–loss function [12] to compute aerodynamic loads of each blade section. For each flight condition, the aerodynamic solver yields the estimated thrust (T) and power (P) given by the selected blade. To compute the performance of the blade operating in one flight condition, it is necessary first to calculate the corresponding trim condition of the rotor (in terms of pitch blade angle ϕ_{trim}, see Ref. [7]). Fixed the blade shape and the flight condition (from which the reference conditions can be extracted, RC_k^{∞}, $k = 1, 2, 3,$), the trim condition can be computed with the BEMT operator ($\mathbb{B}$). Since the calculation of the trim condition can be fundamental to the evaluation of the blade performance for a given flight condition, trim pitch angle is computed by the BEMT operator ($\mathbb{B}$) in order to satisfy the thrust required constraint (T_r).

In order to have good results in relatively short computational time, it has been decided to use a population size of 70 individuals per generation. At each iteration, the solver combines the previous population with an offspring population that is the result of binary tournament selection, recombination and mutation operators. The resultant population is then sorted according to a fast nondomination procedure and members of new population are selected with a fast crowded distance estimation procedure that uses the crowded–comparison operator (see Ref. [6]). To start the optimization procedure an initial population is required. Poles, Fu and Rigoni (see Ref. [13]) have shown that, if genetic information present in the initial population is not enough, the genetic algorithm can converge prematurely to a local optimal solution. Such problem can be fixed making use of a well–distributed initial population. Deb (see Ref. [10]) suggests to include in the initial population some feasible individuals already known. For these reasons, before starting the multi–objective optimization, single objective constrained optimizations have been carried out for each objectives defined before in the paper. Therefore, the initial population for the multi–objective optimization has been created selecting individuals form each final populations of single objective optimizations. The optimization procedure ended when the NSGA–II reached the convergence near the Pareto–optimal front.

3.2 Optimization results

Single objective optimizations gave individuals that show very good performance in their optimization condition. At the same time, these individuals showed very poor performance in other flight conditions. For example, single objective optimization yelded for hovering rotor (condition 1) an optimum individual characterized by a FM of 0.706, while in cruise flight (condition 3) the same individual showed an η_{cruise} of 0.379. In the same way, optimum individual for flight condition 3, that had η_{cruise} of 0.824, showed a FM of 0.635.

The multi–objective optimization, that had the initial population composed by individuals of final populations of single objective optimizations, ended in 122 iterations (8610 individuals have been evaluated) and the algorithm gives a Pareto–optimal set composed by 25 optimal individuals, fig. 2. To chose the best blade from the Pareto–optimal front, some considerations have been done. First of all, individuals that had high values in terms of η_{cruise} showed low capabilities in hovering and climbing flight, while individuals characterized by high values of FM showed low values of η_{cruise}. It has been also observed that individuals with very high values of FM had usually a span–wise twist distribution that limits the propulsive efficiencies in high–speed cruise flight. Hence, the resulting blade is a compromise solution between all the solutions of the Pareto–optimal set. Geometrical characteristics of the blade are shown in tab. 4 and its planform has been reported in fig. 3. In tab. 4, the twist angle θ along the span of the blade is defined as the angle between the hub plane and the section chord (positive nose up) with null collective pitch. Each section has been rotated around an axix passing through 0.25% of local chord. Since in high speed cruise flight, the larger part of the blade operates at higher subsonic and transonic Mach numbers, the leading edge of the blade has been sweeped to reduce power losses due to onset of compressibility losses. A progressive sweep angle has been designed adopting the incident Mach number criterion (see. [7] and [8]). The resulting longitudinal positions ($\Delta x/R$) of sections are reported in tab. 4.

Sec	c/R	θ (deg)	$\Delta x/R$	Airfoil
1	0.131	9.061	0.000	NACA 0030
2	0.133	8.351	0.000	NACA 0020
3	0.144	8.324	0.000	NACA 23014
4	0.168	5.217	0.003	VR–5
5	0.179	-0.005	0.017	OA–213
6	0.155	-2.265	0.025	VR–7
7	0.154	-2.849	-0.003	VR–5
8	0.131	-3.540	-0.046	RC–510
9	0.108	-4.759	-0.077	RC–510

Table 4: Geometric characteristics of the blade.

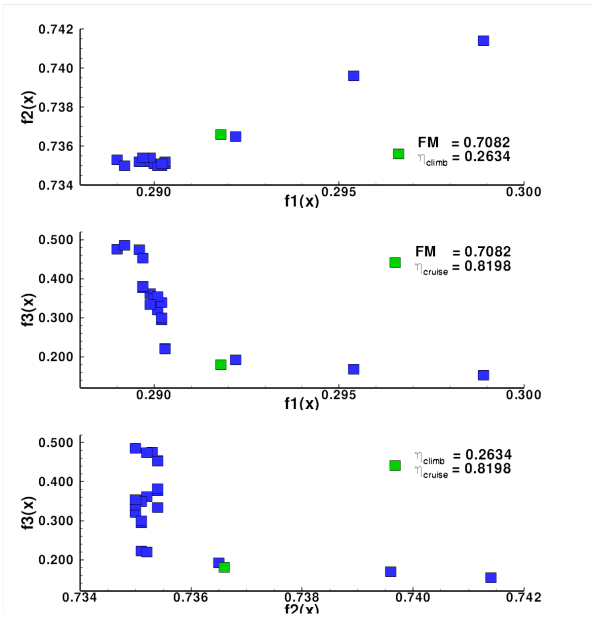

Figure 2: Pareto–optimal front.

Fig. 4 shows the variation of the FM versus the blade loading coefficient (C_t/σ). Increasing the blade loading coefficient, the rotor operates at increasing value of FM. The higher value of FM is reached at $C_t/\sigma = 0.115$. For higher values of blade

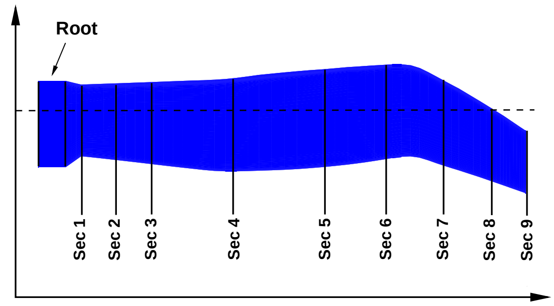

Figure 3: Optimized blade planform.

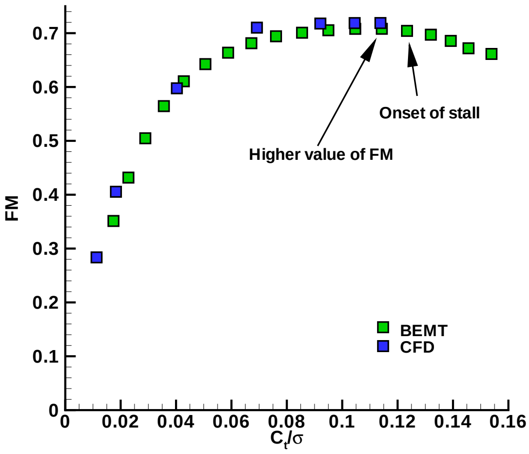

Figure 4: Prediction of FM as function of C_t/σ: comparison between BEMT and CFD calculation.

loading coefficient, the FM decreases by the occurrence of local flow separation on the blade (onset of stall, green squares). In fig. 4 CFD results (blu squares, see chapter 4) for hovering rotor are also showed. Comparison between BEMT and CFD results shows a good agreement in terms of FM versus blade loading coefficient, even though small underpredictions of BEMT calculations should be noted. Figures from 5 to 7 show the variation of thrust, power and propulsive efficiency versus tip speed ration for increasing values of blade pitch angle in cruise flight condition. It can be observed that, ones the the pitch angle is fixed, when the airspeed decreases the blade is stalled and it requires a significant amount of power to get low values of thrust. Instead increasing the airspeed the required power decrease because the flow separation on the blade diminishes, hence η_{cruise} tends to increase. As noted by Leishman and Rosen [8], for high values of airspeed the blade operates in high transonic flow and the progressive growing of compressibility effects give flow separation at the blade tip behind a shockwave. The BEMT is based on section characteristics, thus the predicted blade stall, especially at high local Mach number, may be different from reality. It follows that CFD analyses and experimental mesurements are needed to characterize the blade in these regimes.

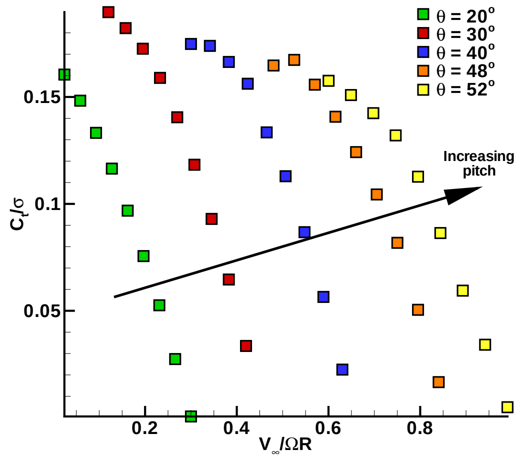

Figure 5: Prediction of thrust as function of tip speed ration for various pitch angles.

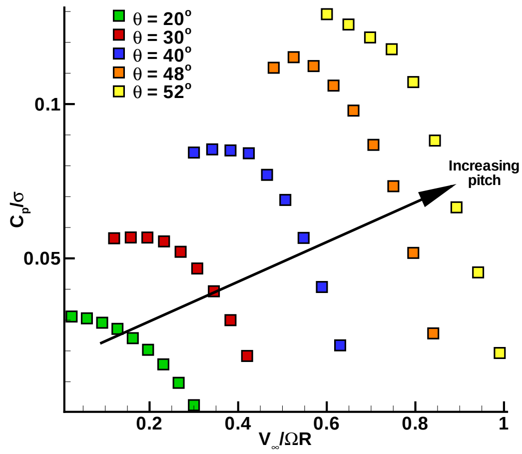

Figure 6: Prediction of power as function of tip speed ration for various pitch angles.

4 Numerical simulation

In the present work, numerical simulations have been used to verify the BEMT calculation during the blade design (see fig. 4). CFD calculations have been carried out also on the whole aircraft to estimate the aerodynamic loads for the experimental test rig design. At the same time, parametric

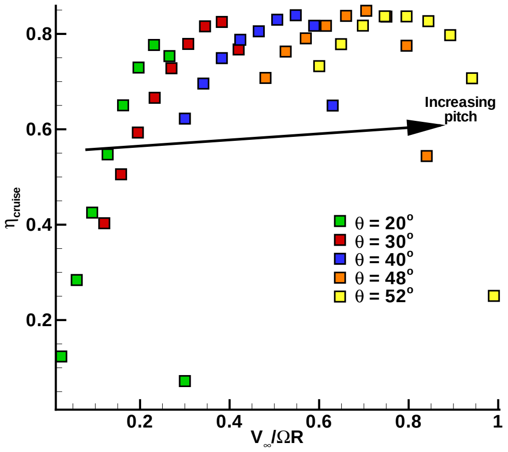

Figure 7: Prediction of propulsive efficiency as function of tip speed ration for various pitch angles.

study has been performed to investigate the phenomena related to wing–rotor aerodynamic interaction in tiltrotor aircraft. In particular, the effects of the span position of the tilt wing section on the tiltrotor performance have been studied. Numerical simulation have been performed with the CFD code ROSITA (ROtorcraft Software ITAly) developed at Politecnico of Milano [14] and [15], based on the solution of the Reynolds Averaged Navier-Stokes (RANS) equations coupled with the one-equation turbulence model of Spalart-Allmaras.

4.1 Description of the CFD code

The CFD code ROSITA [16] numerically integrates the unsteady RANS equations, coupled with the one- equation turbulence model of Spalart–Allmaras [17] and formulated in terms of absolute velocity in overset systems of moving multi–block structured grids. The equations are discretized in space by means of a cell–centred finite–volume implementation of the Roe's scheme [18]. Second order accuracy is obtained through the use of MUSCL extrapolation supplemented with a modified version of the Van Albada limiter introduced by Venkatakrishnan [19]. The viscous terms are computed by the application of the Gauss theorem and using a cell–centred discretization scheme. Time advancement is carried out with a dual–time formulation [20], employing a 2^{nd} order backward differentiation formula to approximate the time derivative and a fully unfactored implicit scheme in pseudo–time. The generalized conjugate gradient (GCG), in conjunction with a block incomplete lower–upper preconditioner, is used to solve the resulting linear system.

The connectivity between the (possibly moving) component grids is computed by means of the Chimera technique. The approach adopted in ROSITA is derived from that originally proposed by Chesshire and Henshaw [21], with modifications to further improve robustness and performance. The domain boundaries with solid wall conditions are firstly identified and all points in overlapping grids that fall close to these boundaries are marked as holes (seed points). Then, an iterative algorithm identifies the donor and fringe points and lets the hole points grow from the seeds until they entirely fill the regions outside the computational domain. To speed up the search of donor points, oct-tree and ADT (alternating digital tree) data structures are employed.

The ROSITA solver is fully capable of running in parallel on computing clusters. The parallel algorithm is based on the message passing programming paradigm and the parallelization strategy consists in distributing the grid blocks among the available processors. Each grid block can be automatically subdivided into smaller blocks by the CFD solver to attain an optimal load balancing.

4.2 Numerical results

The numerical simulations for the isolated blade are performed for all the three flight conditions considered during blade optimization (see 3). The computational mesh is composed of 2 structured multi–block grids, for a total of 9 blocks and $6.27M$ cells (see tab. 5 for details). Calculations have been carried out with a periodic O–H farfield mesh (the external grid), with the outer boundaries located $4R$ away from the blade tip in the span–wise direction, $8R$ above and $18R$ below the rotor plane in vertical direction. The blade mesh (inner grid) has the outer boundary located $1.5R$ from the tip in the span–wise direction and extends vertically by 2, having similar spatial resolution to the first one. Efficient computations for hovering flight condition can be carried out using Froude boundary conditions [15]. Comparisons between CFD calculations and BEMT predictions for the hovering rotor are showed in fig. 4 (see paragraph 3.2). In fig. 8 and 9 the q-criterion visualization for the isolated blade in hovering and cruise flight conditions are reported. While in the hovering condition the tip vortex of the preceding blade interact with the considered blade, in cruise flight there are no significant effects due to this kind of interaction. Small overpredictions of CFD calculations in the FM of hovering rotor (fig. 4), especially for low C_t/σ values, can be due to BVI effects, that are completely neglected in BEMT computations.

The CFD simulations for the whole aircraft have been performed to investigate the phenomena re-

Grid	No. Blocks	No. Nodes ($\times 10^6$)
Blade	8	4.06
Farfield	1	2.21
Total	9	6.27

Table 5: Computational mesh details for isolated blade calculations.

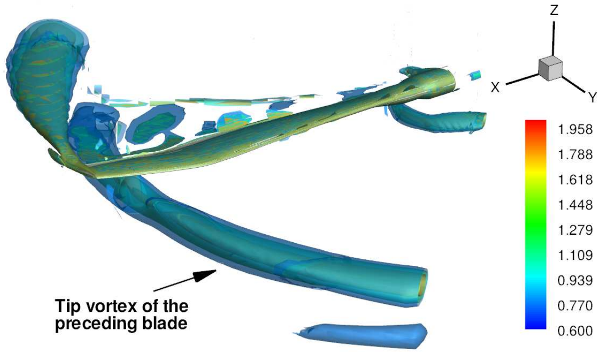

Figure 8: Q-criterion visualization for the isolated blade in hovering flight: $\phi_{trim} = 14°$, $C_t/\sigma = 0.1138$, $FM = 0.7188$.

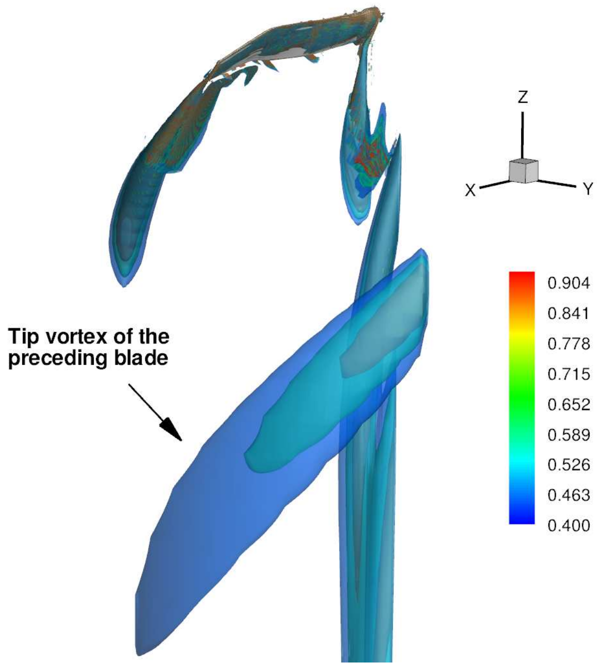

Figure 9: Q-criterion visualization for the isolated blade in cruise flight: $\phi_{trim} = 58°$, $C_t/\sigma = 0.0837$, $C_p/\sigma = 0.1056$, $\eta_{cruise} = 0.8093$.

lated to wing–rotor aerodynamic interaction in tiltrotor aircraft. At this point of the research activity, effects of the span position of the tilt wing section on the tiltrotor performance have been studied and wing download caused by the interaction with the rotor wake in hover and climb conditions have been estimated. In order to define a wing that gives the maximum aerodynamic performance in terms of download in hover, CFD calculations are used to test different wing configurations in terms of span–wise locations of the tilt section. As just mentioned in chapter 2, a half–model configuration (fig. 1) reproducing one half–wing and one rotor with the nacelle have been taken into account. To test 5 different wing configurations (see fig. 10), different grids have been achieved for the 2 wings but the total number of cells was kept constant. In general, the computational mesh is composed by 6 structured multi–block grids, for a total of 48 blocks and $13.35M$ cells (see tab. 6 for details on configuration 2). With the aim to limit the total number of cells, the background grid is composed by 2 different grids, one fine (the inner grid, farfield 1) and one coarse (the outer grid, farfield 2). All the other grids are contained inside the finest background grid, having similar spatial resolution. In fig. 12 multi–block oversetting grids of wings, nacelle and actuator disk are represented. In fig. 13 and 14 some details of the resultant grid are shown. The grids of wings and nacelle are C grid, with the outer boundaries located $0.4R$ away from the bodies except in the wake direction where the boundaries are located $1.6R$ from the trailing edge. Since the root of the fixed wing (wing 1) lies on the aircraft symmetry plane, a symmetry condition has been applied to that plane, whereas both wings and the nacelle have been modelled through no-slip boundary conditions. Because of need of many different simulations, in this phase of the activity it has been decided to save computational time performing steady simulations and reproducing the effects of the rotor with an actuator disk. The actuator disk model embedded in ROSITA follows the Momentum Theory without simulationg the swirl effect due to the blade rotation. Anyway, this kind of approximation can be accepted at this stage. The actuator disk grid, that is an O–H grid, models a disk without thickness in which a jump of pressure is given. The pressure distribution on the disk, for both hovering and climbing flight conditions, has been computed from knowledge of the axial load distribution on the blade (CFD calculations).

Results for 5 different wing configurations, plus the non–realistic configuration with both wings tilted, for hovering and climbing flight conditions are shown in the following. In reference to fig. 10, in fig. 11 download estimations for every tested configuration are displayed. From fig. 11 it is quite clear that configurations 1 and 2 give better results than other configurations in both fligh modes. In these 2 configurations, the rotor wake strikes only on tilted wing surface without any significat interaction with the fixed wing. Also configuration 3

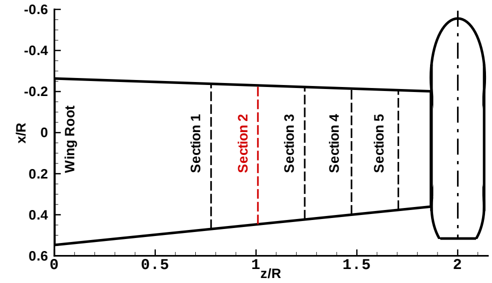

Figure 10: Different tilt wing configurations.

gives good results in terms of download in hover, but some interactions between rotor wake and wings arise near the tilt section. Configurations 4 and 5, in which the tilt wing span is significant smaller than the rotor radius, interaction between wing and rotor becomes more relevant giving higher download values for both hovering and climbing flight conditions. Examples of flow fields in terms of Mach number distribution in a plane parallel to the thrust direction in each configuration are given in fig. from 15 to 20. From CFD analyses configuration 2 seems to give the best compromise in terms of aerodynamic interaction between rotor and wing, hence configuration 2 has been selected for the test rig design.

Grid	No. Blocks	No. Nodes ($\times 10^6$)
Wing 1	7	2.13
Wing 2	9	2.93
Nacelle	25	5.21
Actuator Disk	1	0.29
Farfield 1	1	1.95
Farfield 2	5	0.84
Total	48	13.35

Table 6: Computational mesh details for half–aircraft calculations (configuration 2).

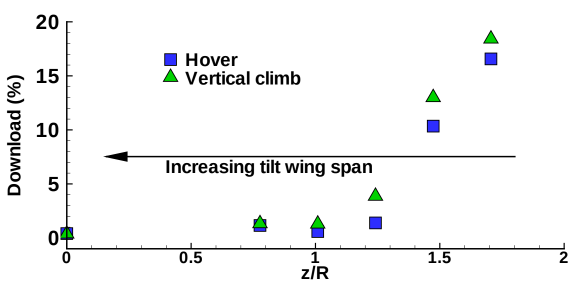

Figure 11: Download distribution as function of tilt wing span for hovering and climbing flight.

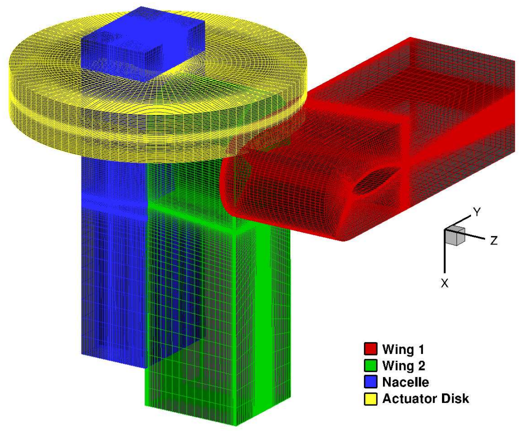

Figure 12: An example of oversetting grids for hovering and climbing flight for CFD calculation.

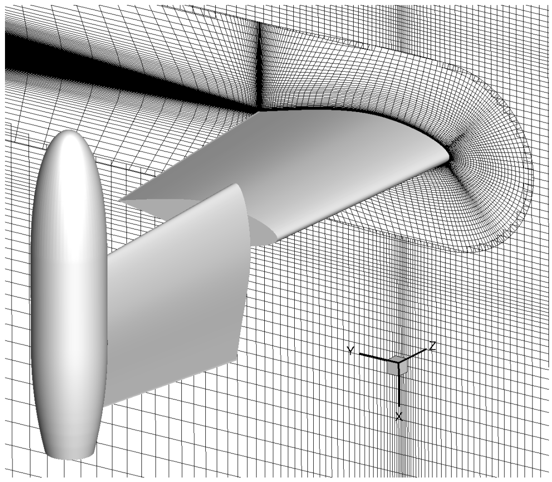

Figure 13: An example of grids system for hovering and climbing flight for CFD calculation.

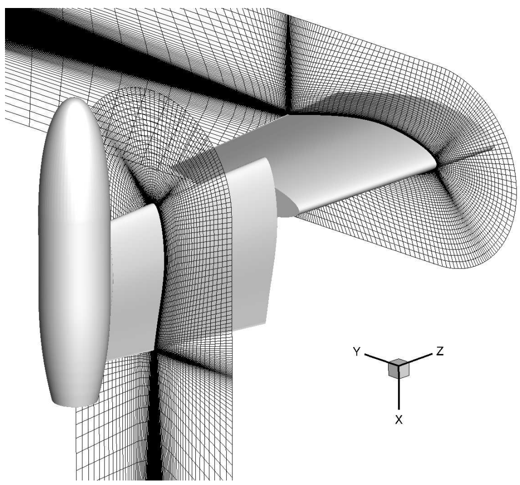

Figure 14: An example of grids system for hovering and climbing flight for CFD calculation.

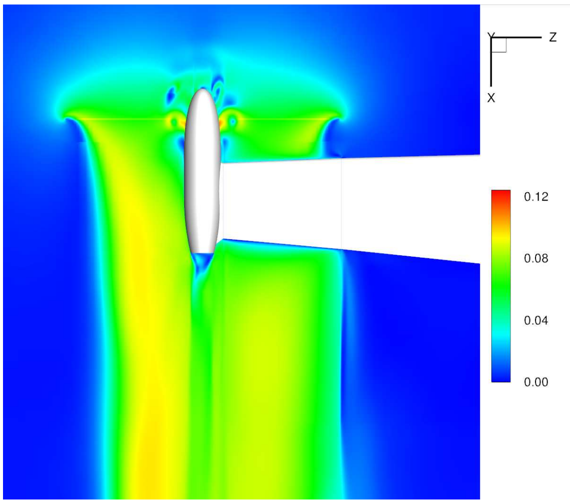

Figure 15: Mach distribution, configuration 0.

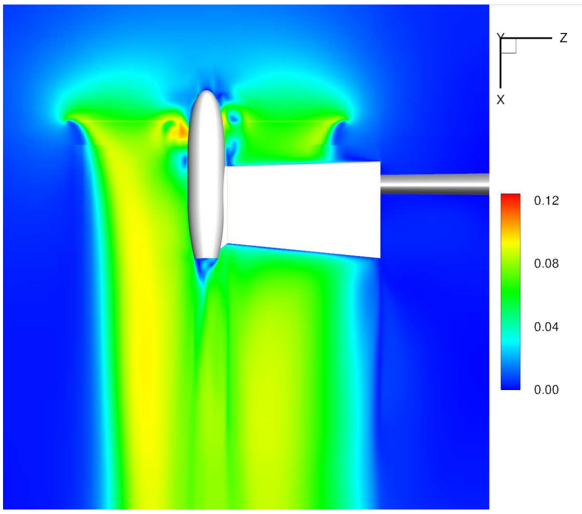

Figure 16: Mach distribution, configuration 1.

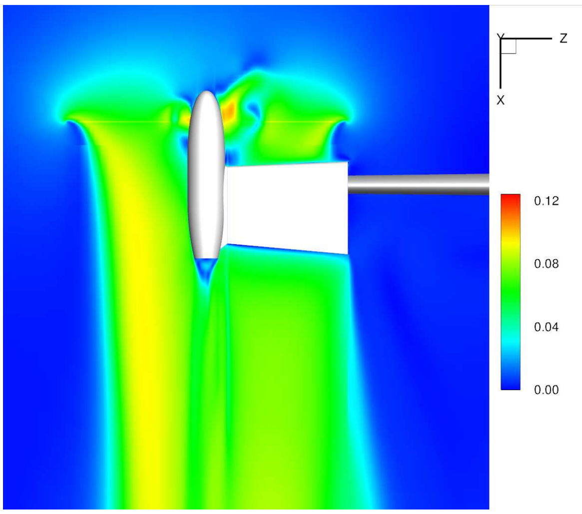

Figure 17: Mach distribution, configuration 2.

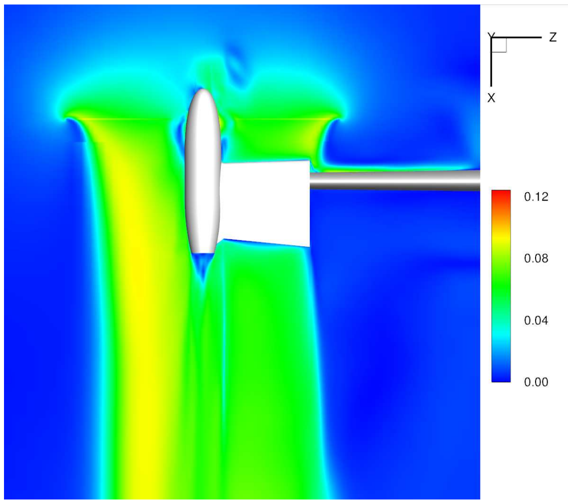

Figure 18: Mach distribution, configuration 3.

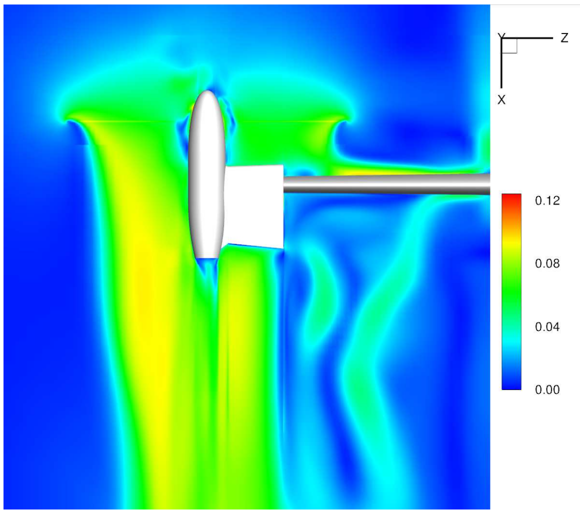

Figure 19: Mach distribution, configuration 4.

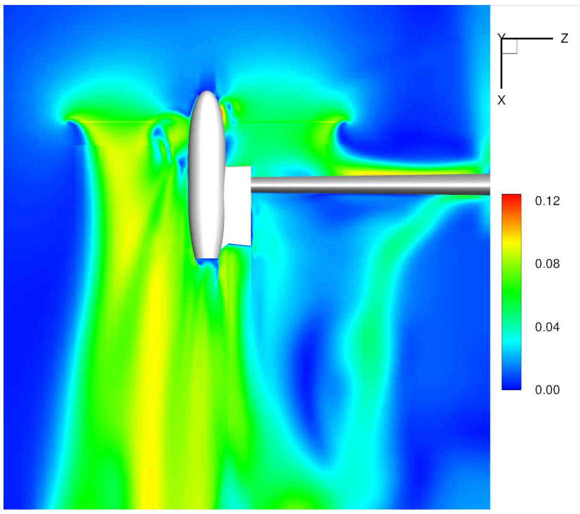

Figure 20: Mach distribution, configuration 5.

5 Conclusions

Aerodynamic interaction between wing and rotors of a tiltrotor aircraft can produce negative effects on its flight performance. Furthermore there are some quite basic aspects of the aerodynamics of wing–rotor interaction that could be studied more deeply for future evolutions. A research activity about the aerodynamic wing–rotor interference was started at Politecnico of Milano. In the first part of the activity, the blade geometry has been designed making use of multi–objective optimization and CFD calculations have been performed to validate optimization results. CFD simulations are also used to estimate the wing download caused by the interaction with the rotor wake in hover and climb flight conditions. Five wing configurations have been tested for different span–wise locations of the tilt section and the configuration which gives the maximum aerodynamic performance in terms of download has been selected. Numerical simulations have also been used to estimate the aerodynamic loads on the wings and to help the design of an experimental test rig. A first release of the model (see fig. 21) has been realized making wide use of pre-existing components some of which will be refined in the course of the activity. In the starting phase of the activity the tests will be limited to the hovering flight condition. In the future, a further evolution of this rig will allow for wind tunnel tests of both helicopter mode forward flight and aircraft mode flight.

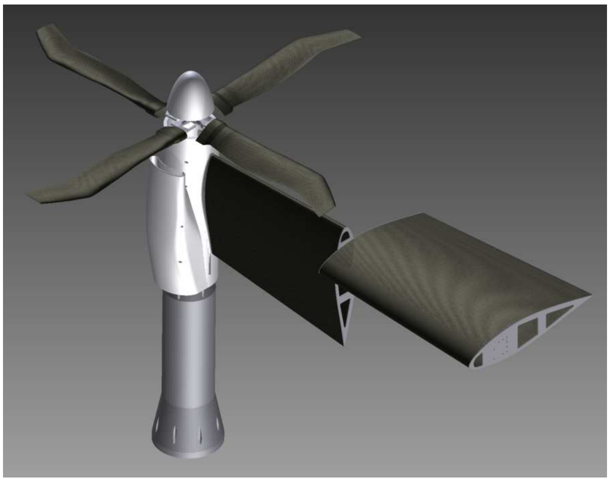

Figure 21: Experimental model for hovering tests.

References

[1] McVeigh, M. A., "The V–22 Tiltrotor Large–Scale Rotor Performance/Wing Download Test and Comparison With Theory," *Vertica*, Vol. 10, No. 3/4, 1986, pp. 281–297.

[2] Felker, F., "Wing Download Results from a Test of a 0.658-Scale V–22 Rotor and Wing," *Journal of the American Helicopter Society*, October 1992, pp. 58–63.

[3] Alli, P., Nannoni, F., and Cicalè, M., "Erica: The european tiltrotor design and critical technology projects," *AIAA/ICAS*, International Air and Space Symposium and Exposition: The Next 100 Years, Day-ton, Ohio, USA, 14–17 July 2005.

[4] Roskam, J., *Aircraft design*, Roskam Aviation and Engineering Corporation, Rt4, Box 274, Ottawa, Kansas, 66067, USA, 1985.

[5] Torenbeek, E., *Synthesis of Subsonic Airplane Design*, Delft University Press, Rotterdam, Netherlands, 1976.

[6] Deb, K., "A fast and elitist multiobjective genetic algorithm: NSGA-II," *IEEE Transactions on Evolutionary Computation*, Vol. 6, No. 2, April 2002, pp. 182–197.

[7] Leishman, J. G., *Principles of Helicopter Aerodynamics*, Cambridge Aerospace Series, New York, NY 10013–2473, USA, 2006.

[8] Leishman, J. G. and Rosen, K. M., "Challenges in the Aerodynamic Optimization of High-Efficiency Proprotors," *Journal of the American Helicopter Society*, Vol. 56, No. 1, January 2011, pp. 12004–1200421.

[9] Maisel, M., Giulianetti, D., and Dugan, D., "The history of the XV-15 tilt rotor research aircraft: from concept to flight," Monographs in Aerospace History, 17 SP-2000-4517, NASA History Division, Washington, D.C., USA, 2000.

[10] Deb, K., *Multi–objective optimization using evolutionary algorithms*, John Wiley and Sons Ltd, Southern Gate, Chichester, West Sussex, United Kingdom, 2008.

[11] Glauert, H., *Airplane Propellers, Division L of Aerodynamic Theory*, Springer Verlag, Berlin, Germany, 1935.

[12] Goldstein, L., "On the Vortex Theory of Screw Propellers," *Proceedings of the Royal Society of London. Series A, Containing Papers of a Mathematical and Physical Character*, Vol. 123, No. 792, 1929, pp. pp. 440–465.

[13] Poles, S., Fu, Y., and Rigoni, E., "The Effect of Initial Population Sampling on the Convergence of Multi–Objective Genetic Algorithms," *Multiobjective Programming and Goal Programming: Theoretical Results and Practical Applications*, Vol. 618, No. 3, 2009, pp. pp. 123–133.

[14] Biava, M., Boniface, J.-C., and Vigevano, L., "Influence of wind–tunnel walls in helicopter aerodynamics predictions," 31^{st} European Rotorcraft Forum, Florence, Italy, 13–15 September 2005.

[15] Biava, M., *RANS computations of rotor/fuselage unsteady interactional aerodynamics*, Ph.D. thesis, Politecnico di Milano, 2007.

[16] Biava, M., Pisoni, A., Saporiti, A., and Vigevano, L., "Efficient rotor aerodynamics predictions with an Euler method," 29^{th} European Rotorcraft Forum, Friedrichshafen, Germany, 16–18 September 2003.

[17] Spalart, P. and Allmaras, S., "One equation model for aerodynamic flows," *AIAA 92-0439*, 30^{th} AIAA Aerospace Science Meeting & Exhibit, Reno, Nevada, USA, 1992.

[18] Roe, P. L., "Approximate Riemann Solvers, Parameter Vectors and Difference Schemes," *Journal of Computational Physics*, Vol. 43, 1981, pp. 357–372.

[19] Venkatakrishnan, V., "On the accuracy of limiters and convergence to steady state solutions," *AIAA 1993–880*, 31^{st} AIAA Aerospace Science Meeting & Exhibit, Reno, Nevada, USA, 1993.

[20] Jameson, A., "Time Dependent Calculations Using Multigrid with Applications to Unsteady Flows past Airfoils and Wings," *AIAA 91–1596*, 10^{th} AIAA Computational Fluid Dynamics Conference, Honolulu, HI., 1991.

[21] Chesshire, G. and Henshaw, W. D., "Composite overlapping meshes for the solution of partial differential equations," *Journal of Computational Physics*, Vol. 90, 1990, pp. 1–64.